Arabian Journal of Chemistry (2022) **15**, 104057

King Saud University

Arabian Journal of Chemistry

www.ksu.edu.sa
www.sciencedirect.com

ORIGINAL ARTICLE

Bioassay and UPLC-Q-Orbitrap-MS/MS guided isolation of polycyclic polyprenylated acylphloroglucinols from St. John's wort and their neuroprotective activity

Huayong Lou [a,b], Fengwei Ma [a,b], Ping Yi [a,b], Zhanxing Hu [a,b], Wei Gu [a,b], Liejun Huang [a,b], Wenwen He [a,b], Chunmao Yuan [a,b,*], Xiaojiang Hao [a,b,c,*]

[a] *State Key Laboratory of Functions and Applications of Medicinal Plants, Guizhou Medical University, Guiyang 550014, China*
[b] *The Key Laboratory of Chemistry for Natural Products of Guizhou Province and Chinese Academy of Sciences/Guizhou Provincial Engineering Research Center for Natural Drugs, Guiyang 550014, China*
[c] *State Key Laboratory of Phytochemistry and Plant Resources in West China, Kunming Institute of Botany, Chinese Academy of Sciences, Kunming 650201, China*

Received 11 May 2022; accepted 14 June 2022
Available online 18 June 2022

KEYWORDS

St. John's wort;
Dietary supplement;
Polycyclic polyprenylated acylphloroglucinols;
Hyperforen A;
Neuroprotective effects

Abstract St. John's wort (*Hypericum perforatum* L.) is a popular dietary supplement ingredient used for the treatment of mild-to-moderate depression in the United States and Germany. Reported studies mainly focused on the biological evaluation and mechanism study of its crude extracts or two main components (namely, hypericin and hyperforin). However, it is unclear whether other phytochemicals including polycyclic polyprenylated acylphloroglucinols (PPAPs) contributed to the neuroprotective effects of *H. perforatum*. Here, bioassay and ultra performance liquid chromatography–quadrupole orbitrap mass spectrometry (UPLC-Q-Orbitrap-MS/MS) guided isolation were applied to discover bioactive PPAPs from the crude extracts of *H. perforatum*. A new PPAP, named hyperforen A (**2**), along with nine known PPAPs (**1** and **3**–**10**), were identified from an ethyl acetate extract of *H. perforatum*. To the best of our knowledge, compound **2** represents the first PPAP with an unprecedented bicyclo[7.3.0]dodecane core. The chemical structures of the isolates were elucidated by extensive spectroscopic analysis and electronic circular dichroism calculations. Moreover, compounds **1**–**3**, **6**, and **10** (10 μM) exhibited significant neuroprotective effects against corticosterone-induced injury in PC12 cells. Fingings from the current study suggest that

* Corresponding author.
E-mail addresses: yuanchunmao01@126.com (C. Yuan), haoxj@mail.kib.ac.cn (X. Hao).
Peer review under responsibility of King Saud University.

Production and hosting by Elsevier

https://doi.org/10.1016/j.arabjc.2022.104057

bioactive PPAPs from *H. perforatum* are promising compouds for the management of depression.

1. Introduction

Depression is a neuropathological disorder that affects 3.8% of the global population (Evans-Lacko et al., 2018). Multiple factors, including genetic, environmental, and psychological factors, contribute to the progression of this disease. Although a variety of antidepressants have been approved by the United State food and drug administration (FDA), those medications are associated with many side effects, such as nausea, vomiting, and sleep disturbances (FDA, https://www.fda.gov/consumers/consumer-updates/depression-fda-approved-medications-may-help). Although the pathogenesis of depression is not fully elucidated, numerous studies suggest that it is associated with the decrease and damage of hippocampal neuron cells (Sapolsky, 2000; Kim et al., 2018). It is of great interest to search for neuroprotective natural products with less adverse effects. Abnormal high levels of corticosterone (CORT), a principal glucocorticoid, cause hippocampal neuron damage (Cui and Catharina, 2002; Germ et al., 2010) and induce depression-like behaviour in animals, which can be reversed by the anti-depressants (Shadfar et al., 2018; Yang et al., 2012). Thus, the CORT-stimulated PC12 cells model is a well-established neuroprotective model for screening natural products with neuroprotective and anti-depressive effects (Zhou et al., 2016; Jiang et al., 2014).Fig. 1..

Hypericum perforatum L., also known as St. John's wort (SJW), is commonly distributed worldwide. Its extracts are consumed as a dietary supplement to manage mild-to-moderate depression in the United States and Germany (Laakmann et al., 1998; Bruni et al., 2005). Many SJW products are used as dietary supplements in Europe and the United States, such as GNC St. John's Wort Extract Capsules, Solaray St. John's Wort Dietary Supplement, and Swisse Mood Tablets (Hou et al., 2020). In addition, SJW extracts are used as ingredients in several functional foods, beverages, and yogurts (Ang et al., 2004; Germ et al., 2009).

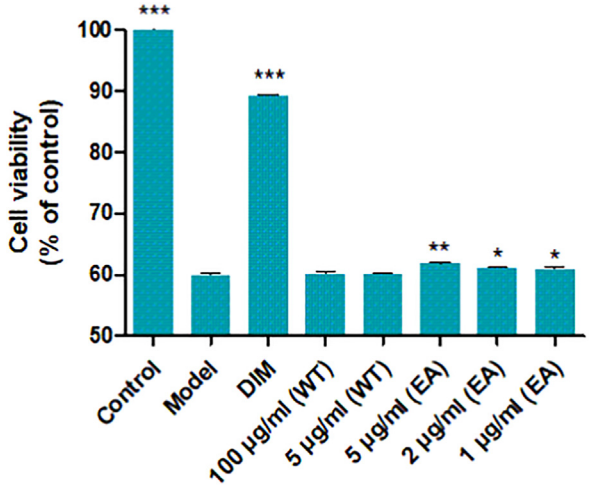

Fig. 1 The water (WT) and ethyl acetate (EA) parts for CORT-induced injury in PC12 cells. ***$P < 0.001$, **$P < 0.01$, *$P < 0.05$ *vs.* model.

Recent pharmacological studies showed that SJW extracts can exert numerous bioactivities, including anti-inflammatory (Hammer et al., 2007), antioxidant (Zou et al., 2004), antibacterial, wound healing (Besen et al., 2017), and anti-depressive effects. Phytochemical investigation revealed that SJW is rich in naphthodianthrones (Cui et al., 2002), polycyclic polyprenylated acylphloroglucinols (PPAPs) (Guo et al., 2017), flavones (Wilhelm et al., 2001), and fatty acids (Hosni et al., 2017). Among these phytochemicals, hypericin and hyperforin are the major active constituents with promising anti-depressant activity (Cervo et al., 2002). Moreover, many papers focused on the biological activities and mechanism study of SJW crude extracts or hypericin and hyperforin. However, other neuroprotective effects of PPAPs from SJW in depression-related models are not clear.

Separation of designated secondary metabolites from a botanical crude extract requires intense laborious work. Therefore, high-efficiency analytical methods are critical for targeted isolation (Ma et al., 2021; Li et al., 2022). Ultraperformance liquid chromatography-electrospray ionization-mass spectrometry (UPLC-ESI-MS) can generate fragmentation spectra to provide information on the structure scaffolds and facilitate the identification of analogues from a complex matrix (Ma et al., 2016; Chen et al., 2022). Mass spectrometry (MS) relies upon its modularity by coupling to liquid chromatography (LC), which has become an important method for identifying and analysing the chemical constituents of plant extracts (Hsu, 2021).

Here, bioassay and UPLC-Q-Orbitrap-MS/MS guided isolation were applied in the current study. Ten PPAPs (**1**–**10**), including a novel compound with an unusual bicyclo-9/5-fused carbocyclic core skeleton (**2**), were isolated from an ethyl acetate extract of SJW. To the best of our knowledge, compound **2** represents the first PPAP with an unprecedented bicyclo[7.3.0]dodecane core and the largest carbocyclic system. Biogenetically, the architecture of compound **2** might be generated from a known compound (**1**) *via* successive rearrangements involving Westphalen and Wagner-Meerwein rearrangements. Moreover, compounds **1**–**3**, **6**, and **10** (10 μM) exhibited promising neuroprotective effects against CORT-induced cellular injury in PC12 cells. Herein, we report the bioassay and UPLC-Q-Orbitrap-MS/MS guided isolation, structure elucidation, plausible biosynthetic pathway, and the bioactivity of the isolates.

2. Experimental

2.1. Reagents and materials

2.1.1. Chemical

We purchased analytical grade petroleum ether, ethyl acetate, dichloromethane, acetone, and methanol from General-

reagent Corporation (Shanghai, China). High-performance liquid chromatography (HPLC) grade acetonitrile, methanol, and water were purchased from Xinlanjing International Corporation (Pennsylvania, USA). Dulbecco's Modified Eagle Medium (DMEM) and fetal bovine serum (FBS) were obtained from GIBCO Invitrogen Corporation (Carlsbad, USA). DMSO, streptomycin, penicillin, corticosterone (CORT), and 3-(4,5-dimethylthiazol-2-yl)-2,5-diphenyltetrazo lium bromide (MTT) were bought from Sigma-Aldrich (USA).

2.1.2. General experimental procedures

Optical rotation was measured on Autopol-VI for compound **2** at 20 °C. Infrared radiation (IR) spectrum of compound **2** was obtained on a Nicolet Is10 FT-IR spectrometer with KBr pellets. A Shimadzu UV-2401PC spectrometer was applied to record ultraviolet (UV) spectrum of compound **2** at room temperature. An Applied Photophysics Chirascan spectrometer was used to acquire Circular Dichroism (CD) spectrum of compound **2**. ^{1}H (600 MHz) and ^{13}C (150 MHz) NMR (nuclear magnetic resonance) spectra for compounds **1**–**10** were recorded on a Bruker Avance III 600 MHz spectrometer with TMS as internal standard. The HMQC (heteronuclear multiple quantum correlation), HMBC (heteronuclear multiple bond correlation), ^{1}H−^{1}H COSY (correlation spectroscopy), and ROESY (rotating frame overhauser effect spectroscopy), spectra for compound **2** were also acquired on a Bruker Avance III 600 MHz spectrometer. High resolution electrospray ionization mass spectroscopy (HR-ESI-MS) data of compound **2** was acquired on an Agilent 6500 QSTAR Q-Exactive Orbitrap mass spectrometer. Semi-preparative HPLC was carried out on a Waters-C600 with a Waters C18 column (150 mm × 10 mm, 10 μm). Column chromatography was performed using silica gel (40–80, 200–300, and 300–400 mesh, Qingdao Marine Chemical Co. Ltd., Qingdao, People's Republic of China), MCI gel (75–150 μm, Mitsubishi Chemical Corporation, Japan), and Sephadex LH-20 (25–100 μm, Amersham Biosciences, Sweden), respectively.

2.1.3. Plant material

The aerial parts of *H. perforatum* were collected in 2017 from Leishan county, Guizhou Province, China. The plant was identified by Dr. Wei Gu, and a voucher specimen was deposited in the Key Laboratory of Chemistry for Natural Products of Guizhou Province and Chinese Academy of Sciences, Guiyang, China (the voucher specimen: No. 20170321).

2.2. UPLC-Q-Orbitrap-MS/MS-guided isolation

2.2.1. UPLC-Q-Orbitrap-MS/MS

The chromatographic analysis was performed on a Thermo Scientific Dionex (Sunnyvale, USA) Ultimate 3000 UHPLC system equipped with an Ultimate 3000 Pump, an Ultimate 3000 Degasser, an Ultimate 3000 RS Autosampler, and an Ultimate 3000 RS column compartment. The samples were separated using a Hypersil GOLDTM C18 column (3.0 μm, 2.1 × 150 mm; Thermo Fisher Scientific, Waltham, MA, USA). The mobile phase consisted of methanol (A) and water (B). The flow rate was 0.2 mL/min, the column temperature was set at 40 °C, and the total run time was 30 min. An isocratic mode of 70% phase A was applied for 0 ∼ 3 min, followed with a linear gradient from 70% to 100% phase A between 3 and 25 min, and 100% phase A was maintained over the last 5 min.

Mass spectrometry with an electrospray ionization source (ESI) was conducted in the positive mode. High-resolution ESI-MS/MS experiments were performed on a Q-Exactive Orbitrap mass spectrometer equipped with an ESI source controlled by the Xcalibur 2.3 software (Thermo Fisher, Waltham, MA, USA). The mass resolution was 17,500 FWHM (full width at half maximum) at 200. Argon was used as the collision gas, and high-purity nitrogen gas was used as the nebulizer and drying gas was set at a flow rate of 4 L/min and a pressure of 0.3 bar, respectively. The heated electrospray ion source was used for the ionization with the interface conditions were as follows: spray voltage, 3.0 kV; and capillary temperature, 320 °C; sheath gas flow rate, 35 units; auxiliary gas flow rate, 10 units; and S lens RF level 50.

2.2.2. Isolation and purification

The air-dried aerial parts (8.8 kg) of SJW were smashed to powders (10–50 mesh), which were further percolated extract with MeOH at room temperature for three times (40 L × 3) and then filtered. The combined MeOH extracts were concentrated under vacuum to give a crude residue (495.0 g), which was suspended in water and then partitioned successively with ethyl acetate (EA) to get the corresponding extracts: EA (150.0 g) and water (WT) (300.0 g) parts. Both EA and WT fractions were screened for the neuroprotective activity (Fig. 1). The active EA fraction was further separated by silica gel column chromatography and eluted with petroleum ether-ethyl acetate (from 1:0 to 0:1) to obtain a high content PPAP (**1**, 5 g) and eight fractions (Frs. A–H). This known PPAP (**1**) was an active PPAP after biological test.

Compound **1** was used as a referenced compound and applied to UPLC-Q-Orbitrap-MS. Eight fractions (Frs. A–H) were further analysed using UPLC-Q-Orbitrap-MS. Fraction A of EA extract might have PPAPs according to the results of UPLC-Q-Orbitrap-MS analysis. Therefore, Fr. A (65.1 g) was subjected to column chromatography and eluted with petroleum ether-ethyl acetate (100:1 to 1:1) to obtain seven fractions (Fr. A1–A7). Fr. A3 was further purified by semi-preparative HPLC (MeOH-H_2O, 95:5) to yield compounds **9** (5.2 mg, t_R = 32 min) and **10** (16.3 mg, t_R = 28.4-min). Fr. A4 (32.5 g) was applied to a silica gel column eluted with petroleum ether-acetone (50:1 to 1:1) to yield compound **3** (1.0 g) and five fractions (Frs. A4A–A4E). Fr. A4C (4.8 g) was purified by semi-preparative HPLC (CH_3CN-H_2O, 90:10) to obtain compounds **2** (3.6 mg, t_R = 19.6 min) and **4** (5.2 mg, t_R = 22.8 min). Fr. A5 (10 g) was then separated over an MCI-gel column (MeOH-H_2O from 7:3 to 10:0) to yield seven fractions (Frs. A5A–A5G). Fr. A5G (116 mg) was further purified by semipreparative HPLC (MeOH-H_2O, 85:15) to afford compounds **5** (9.4 mg, t_R = 34.1 min), **6** (11.3 mg, t_R = 27 min), **7** (8.2 mg, t_R = 29.5 min), and **8** (50 mg, t_R = 37.6 min).

*2.2.2.1. Hyperforen A (**2**).* Colorless oil, $[\alpha]_D^{20}$ + 9.53 (*c* 0.05, MeOH); UV (MeOH) λ_{max} (log ε) 201 (3.68) nm; CD (MeOH) λ_{max} (Δε) 226 (-0.63), 304 (1.73), 331 (-1.43) nm, IR (KBr) νmax 3439, 2961, 2926, 1731, 1710, 1631, 1464, 1384, 1109 cm^{-1}; ^{1}H and ^{13}C NMR data, see Table 1.; positive

Table 1 Characterization of chemical constituents from Fr. A by UPLC-Q-Orbitrap-MS.

No.	Rt	Elemental Composition ($[M + H]^+$ or $[M + Na]^+$)	Observed mass	Error (ppm)	Elemental composition of product ions ($[M + H]^+$ or $[M + Na]^+$)	Characteristic product ions	Error (ppm)	Neutral loss unit (u)
X1	10.02	$C_{36}H_{54}O_5Na$	589.3486	−2.25	$C_{17}H_{22}O_5Na$	329.1349	−3.21	$C_{19}H_{32}$ (260 u)
X2	10.35	$C_{35}H_{52}O_5Na$	575.3698	−1.64	$C_{16}H_{20}O_5Na$	315.1195	−2.60	$C_{19}H_{32}$ (260 u)
X3	10.42	$C_{35}H_{52}O_5Na$	575.3690	−2.92	$C_{16}H_{20}O_5Na$	315.1195	−2.60	$C_{19}H_{32}$ (260 u)
X4	10.47	$C_{35}H_{52}O_5Na$	575.3695	−2.07	$C_{16}H_{20}O_5Na$	315.1194	−2.79	$C_{19}H_{32}$ (260 u)
X5	10.51	$C_{35}H_{52}O_5Na$	575.3694	−2.17	$C_{16}H_{20}O_5Na$	315.1203	−3.08	$C_{19}H_{32}$ (260 u)
X6	10.57	$C_{35}H_{52}O_5Na$	575.3700	−1.22	$C_{16}H_{20}O_5Na$	315.1194	−2.99	$C_{19}H_{32}$ (260 u)
X7	10.77	$C_{35}H_{52}O_5Na$	575.3702	−0.79	$C_{16}H_{20}O_5Na$	315.1195	−2.60	$C_{19}H_{32}$ (260 u)
X8	10.81	$C_{35}H_{52}O_5Na$	575.3698	−1.64	$C_{16}H_{20}O_5Na$	315.1194	−2.99	$C_{19}H_{32}$ (260 u)
X9	10.88	$C_{35}H_{48}O_5Na$	571.3381	−2.21	$C_{16}H_{16}O_5Na$	311.0882	−2.47	$C_{19}H_{32}$ (260 u)
X10	10.89	$C_{35}H_{53}O_5$	553.3906	3.39	$C_{16}H_{21}O_5$	293.1377	−2.34	$C_{19}H_{32}$ (260 u)
X11	10.92	$C_{35}H_{52}O_5Na$	575.3703	−0.69	$C_{16}H_{20}O_5Na$	315.1194	−2.99	$C_{19}H_{32}$ (260 u)
X12	11.03	$C_{35}H_{48}O_5Na$	571.3359	−6.16	$C_{16}H_{16}O_5Na$	311.0884	−1.98	$C_{19}H_{32}$ (260 u)
X13	11.05	$C_{35}H_{53}O_5$	553.3911	4.27	$C_{16}H_{21}O_5$	293.1379	−1.51	$C_{19}H_{32}$ (260 u)
X14	11.17	$C_{35}H_{52}O_5Na$	575.3692	−2.60	$C_{16}H_{20}O_5Na$	315.1193	−3.28	$C_{19}H_{32}$ (260 u)
X15	11.17	$C_{35}H_{50}O_5Na$	573.3530	−3.63	$C_{16}H_{18}O_5Na$	313.1031	−4.97	$C_{19}H_{32}$ (260 u)
X16	11.20	$C_{35}H_{53}O_5$	553.3907	3.61	$C_{16}H_{21}O_5$	293.1378	−1.92	$C_{19}H_{32}$ (260 u)
X17	11.21	$C_{35}H_{50}O_6Na$	591.3652	−0.64	$C_{16}H_{20}O_5Na$	315.1194	−2.99	$C_{19}H_{30}$ (276 u)
X18	11.30	$C_{35}H_{52}O_5Na$	575.3695	−2.07	$C_{16}H_{20}O_5Na$	315.1194	−2.99	$C_{19}H_{32}$ (260 u)
X19	11.32	$C_{35}H_{50}O_5Na$	573.3695	−2.07	$C_{16}H_{20}O_5Na$	315.1194	−2.99	$C_{19}H_{30}$ (258 u)
X20	11.33	$C_{35}H_{50}O_6Na$	591.3469	−3.84	$C_{16}H_{20}O_5Na$	315.1201	−0.76	$C_{19}H_{32}$ (276 u)
X21	11.33	$C_{29}H_{44}O_3Na$	463.3167	−3.42	$C_{10}H_{12}O_3Na$	203.0677	−0.72	$C_{19}H_{32}$ (260 u)
X22	11.37	$C_{30}H_{44}O_5Na$	507.3023	−4.62	$C_{16}H_{20}O_5Na$	315.1194	−2.99	$C_{14}H_{24}$ (192 u)
X23	11.40	$C_{35}H_{50}O_5Na$	575.3694	−2.28	$C_{16}H_{20}O_5Na$	315.1198	−1.53	$C_{19}H_{32}$ (260 u)
X24	11.43	$C_{35}H_{50}O_5Na$	575.3694	−2.28	$C_{16}H_{20}O_5Na$	315.1194	−2.99	$C_{19}H_{32}$ (260 u)
X25	11.44	$C_{35}H_{50}O_5Na$	575.3696	−1.96	$C_{16}H_{20}O_5Na$	315.1194	−2.99	$C_{19}H_{32}$ (260 u)
X26	11.45	$C_{35}H_{50}O_5Na$	575.3693	−2.38	$C_{16}H_{20}O_5Na$	315.1194	−2.99	$C_{19}H_{32}$ (260 u)
X27	11.48	$C_{35}H_{50}O_5Na$	575.3690	−2.92	$C_{16}H_{20}O_5Na$	315.1196	−2.31	$C_{19}H_{32}$ (260 u)
X28	11.52	$C_{30}H_{44}O_5Na$	507.3062	−3.71	$C_{16}H_{20}O_5Na$	315.1194	−2.99	$C_{14}H_{24}$ (192 u)
X29	11.62	$C_{36}H_{54}O_5Na$	589.3855	−1.44	$C_{17}H_{22}O_5Na$	329.1352	−2.38	$C_{19}H_{32}$ (260 u)
X30	11.64	$C_{35}H_{50}O_5Na$	575.3690	−3.66	$C_{16}H_{20}O_5Na$	315.1194	−2.99	$C_{19}H_{32}$ (260 u)
X31	11.66	$C_{36}H_{54}O_5Na$	589.3854	−1.65	$C_{17}H_{22}O_5Na$	329.1352	−2.38	$C_{19}H_{32}$ (260 u)
X32	11.67	$C_{36}H_{54}O_5Na$	589.3856	−1.34	$C_{17}H_{22}O_5Na$	329.1351	−2.56	$C_{19}H_{32}$ (260 u)
X33	11.67	$C_{35}H_{53}O_5$	553.3907	−1.91	$C_{16}H_{21}O_5$	293.1374	−3.38	$C_{19}H_{32}$ (260 u)
X34	11.74	$C_{36}H_{54}O_5Na$	589.3853	−1.75	$C_{17}H_{22}O_5Na$	329.1349	−3.21	$C_{19}H_{32}$ (260 u)
X35	11.78	$C_{36}H_{54}O_5Na$	589.3855	−1.44	$C_{17}H_{22}O_5Na$	329.1351	−2.56	$C_{19}H_{32}$ (260 u)

HRESIMS: *m/z* 549.3918 $[M + Na]^+$ (calcd for $C_{34}H_{54}O_4Na$, 549.3914).

2.3. Quantum chemical computations

2.3.1. ^{13}C NMR calculation of 2

Conformational searching of **2** was undertaken with the Spartan software using the Merck molecular force field (MMFF) with standard parameters (Hanwell et al., 2012). All conformers were subjected to density functional theory (DFT) geometry optimization at B3LYP/6-31G (d) level of theory in the gas phase using the Gaussian 16 package. Frequency analyses of all optimized conformers were undertaken at the same level of theory to ensure that a Boltzmann distribution $\geq$ 5% were chosen, and then they were initially optimized at B3LYP/6–3 1 + G (d, p) levels in chloroform using the polarizable continuum model (PCM) solvent model in the Gaussian 16 program package (Zhao et al., 2021). The gauge-independent orbital (GIAO) shielding constants of these conformers were converted into unscaled chemical shifts (δ_u) by referencing to tetramethylsilane (TMS) ($\delta_u = \sigma_{TMS} - \sigma_{Cal}$), where the σ_{TMS} was the shielding constant of TMS calculated at the same level. The scaled chemical shifts (δ_s) were computed by the formula $\delta_s = (\delta_u - b)/m$, where m and b are the slope and intercept, respectively. The linear correlation coefficient was calculated to evaluate deviations between the experimental and calculated results (Chen et al., 2020).

2.3.2. ECD calculation of 2

Conformational searching for **2** was obtained from the same method as ^{13}C NMR calculation of **2**. The conformers with Boltzmann-population of over 5% were chosen for electronic circular dichroism (ECD) calculations, and then the conformers were initially optimized at B3LYP/6–31 g (d, p) level in MeOH using the CPCM polarizable conductor calculation model. The theoretical calculation of ECD was conducted in MeOH using Time-dependent Density functional theory (TD-DFT) at the B3LYP/6–31 + g (d, p) level for all conformers of **1**. Rotatory strengths for a total of 30 excited states were calculated. ECD spectra were generated using the program SpecDis 1.71 (University of Würzburg, Würzburg, Germany) and GraphPad Prism 5 (University of California San Diego, USA) from dipole-length rotational strengths by applying Gaussian band shapes with sigma = 0.3 eV (Lou et al., 2018).

2.4. Evaluation of neuroprotective activity

The isolates were dissolved in DMSO at a stock concentration of 300 mM. The final concentration of DMSO in the culture medium never exceeded 0.1% (v/v), and the same concentration was used in control experiment. PC12 cells were maintained in DMEM (GIBCO Invitrogen Corp., Carlsbad, CA, USA) supplemented with 10% fetal bovine serum (FBS), streptomycin (100 μg/mL), penicillin (100 U/mL), and incubated at 5% CO_2 at 37 °C. Cells in the exponential phase of growth were used in all experiments. The experimental tests included the following groups: corticosterone (CORT, 150 μM), CORT (150 μM) plus desipramine (20.0, 10.0, and 5.0 μM), CORT (150 μM) plus the test compounds (20.0, 10.0, and 5.0 μM), and nontreated control. Unless specified otherwise, the cell suspensions were seeded in every well of 96-well culture plates (1×10^4 cells/well, in triplicate) for 24 h and then exposed to medium containing corticosterone (150 μM) in the presence or absence of various concentrations of tested samples for an additional 48 h. Cell viability was examined using a 3-(4,5-dimethylthiazol-2-yl)-2,5-diphenylte trazolium bromide (MTT) assay. In brief, at the final step of each treatment, phosphate-buffered saline (PBS) was employed to gently wash the cells. After washing, 10 μL of MTT (5 mg/mL) was added to each well. After being maintained at 37 °C for 4 h and removing the culture medium, 100 μL of DMSO was added to each well to dissolve the formazan crystals generated by the reaction. A Thermo Multiskan FC microplate reader was utilized to measure the absorbance at 492 nm. Cell viability was indicated in the form of a percentage of the control (Zhou et al., 2016).

2.5. Statistical analysis

The results are expressed as the means ± standard deviation (SD) (n = 3). Statistical analysis was performed by one-way analysis of variance (ANOVA) followed by Tukey's multiple range post hoc test in SPSS statistical software. A statistically significant difference was considered when $P < 0.05$ (Liu et al., 2020).

3. Results and discussion

3.1. Bioassay and UPLC-Q-Orbitrap-MS guided isolation

3.1.1. Bioassay-evaluation of crude extracts and a high content PPAP

The neuroprotective activities for EA extract and WT extract were screened using a CORT-induced PC12 cellular injury model (Fig. 1). The results showed that the EA fraction exhib-

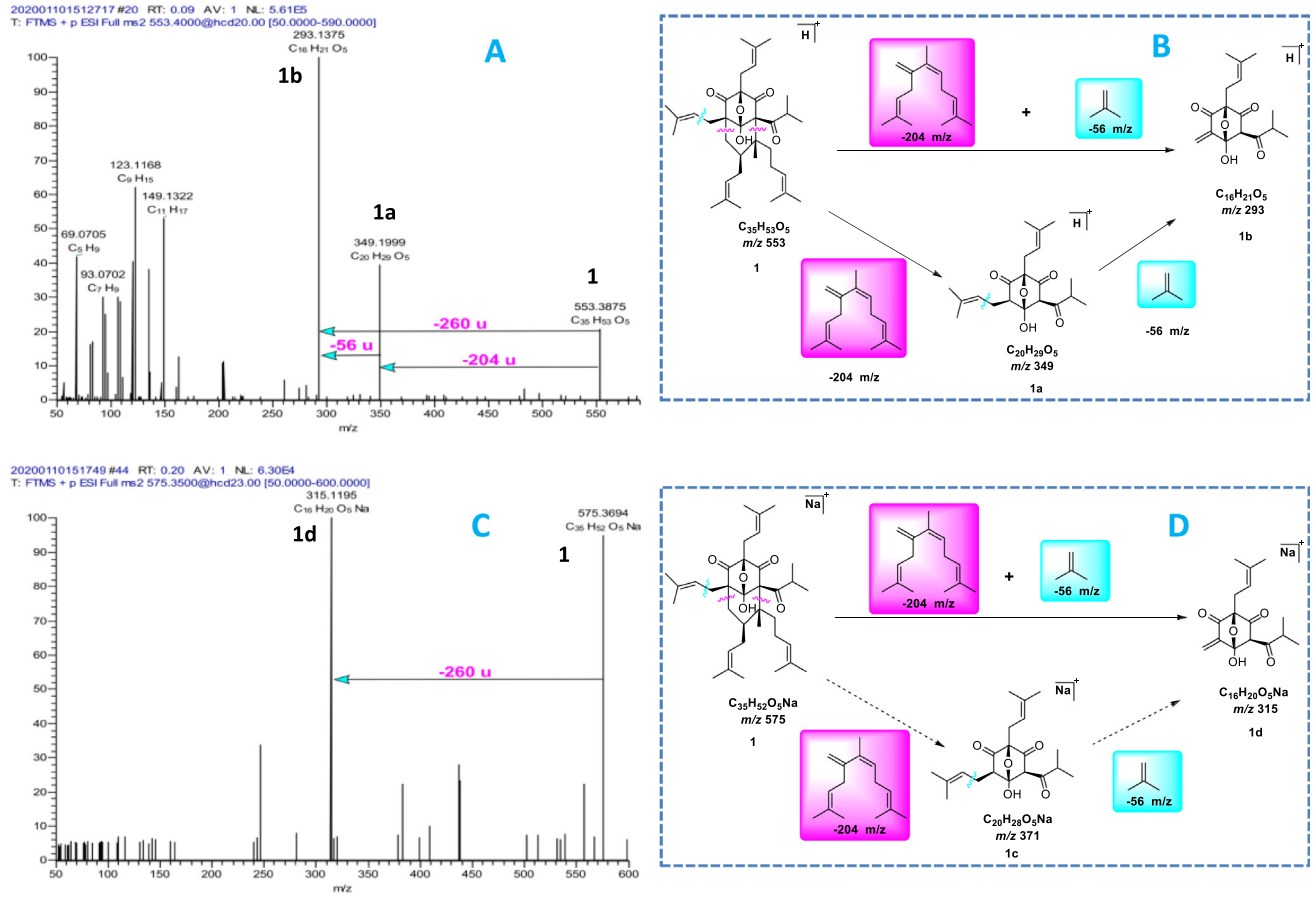

Fig. 2 (A) Product ion scan of the selected precursor $[M + H]^+$ ion at *m/z* 553 for **1** (20% NCE); (B) The proposed major fragmentation patterns of $[M + H]^+$ for **1**; (C) Product ion scan of the selected precursor $[M + Na]^+$ ion at *m/z* 575 for **1** (23% NCE); (D) The proposed major fragmentation patterns of $[M + Na]^+$ for **1**.

ited neuroprotective activity at the concentrations from 1 to 5 μg/ml, while the WT fraction was inactive. The active EA fraction was further separated by silica gel column chromatography to obtain a high content PPAP (**1**, 5 g) and eight fractions (Frs. A–H). Compound **1** (10 μM) was evaluated for the neuroprotective effect and the result indicated that this compound showed a significant protective effect by increasing the injured cell viability to 65.1%.

3.1.2. Characterization of PPAPs from the fractions by UPLC-Q-Orbitrap-MS/MS

PPAPs were considered as the characteristic active chemical constituents in SJW. UPLC-Q-Orbitrap-MS/MS was an important method to identify and analyse the typical chemical constituents of plant extracts. So, a high content compound **1** was used as a referenced compound and was applied to UPLC-Q-Orbitrap-MS/MS. In the mass spectrum, major product ion at *m*/*z* 349 (**1a**) and 293 (**1b**) were detected, which were generated by successive loosing of $C_{15}H_{24}$ (204 u) unit and C_4H_8 (56 u) unit from compound **1** in Fig. 2A. Alternatively, **1b** could be obtained *via* loosing $C_{19}H_{32}$ (260 u) unit from **1** directly (Figure 2B), which is commonly observed with $[M + Na]^+$ ion. As shown in Figure 2C, a major product ion at *m*/*z* 315 (**1d**) was obtained from the precursor $[M + Na]^+$ ion for **1** by loosing of $C_{19}H_{32}$ (260 u) unit (Fig. 2C). Thus, neutral loss of 260 u together with characteristic product ions (293 u, 349 u, 371 u, and 315 u) could be applied for targeted PPAPs detection.

Different fractions (Frs. A–H) obtained from the silica gel column were analysed by UPLC-Q-Orbitrap-MS/MS, and more than 30 analogues (**X1-X35**) were identified or tentatively characterized from fraction A of EA extract, on the basis of their elemental constituents, fragmentation patterns, the product ion profiles, and the neutral loss unit (Table 1 and Figure S2).

3.1.3. Structure elucidation of compounds 1–10

Further isolation for fraction A of the EA extract led to the isolation of 10 PPAPs, including a new PPAP (Fig. 3). By com-

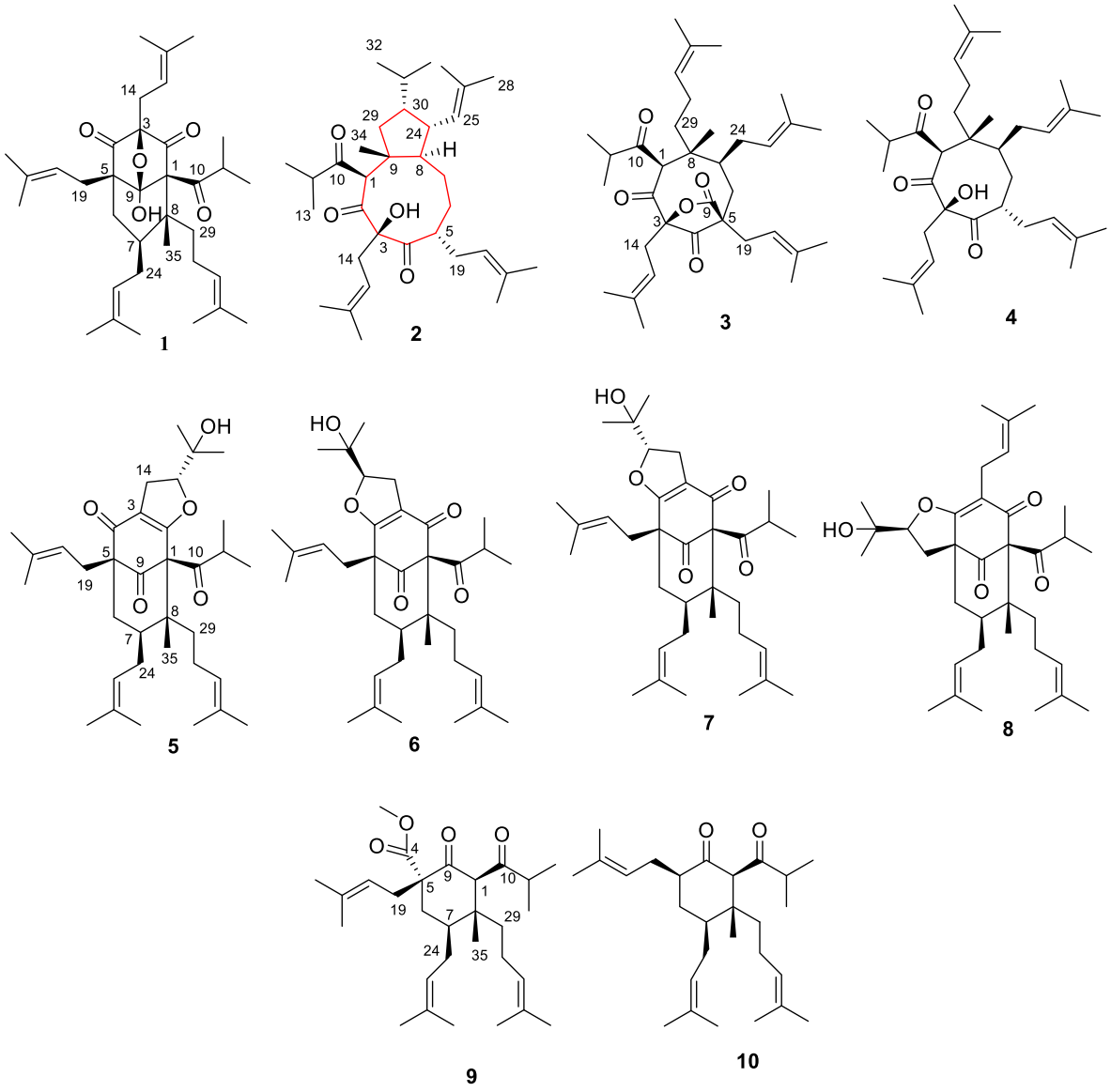

Fig. 3 Chemical structures of **1**–**10**.

parison of the spectroscopic data with those reported in the literature, nine known compounds were identified to be 8-hydro xyhyperforin-8,1-hemiacetal (**1**) (Verotta et al., 2000), hyphenrone A (**3**) (Yang et al., 2014), hyphenrone F (**4**) (Yang et al., 2014), furohyperforin isomer 2 (**5**) (Hashida et al., 2010), 27-epifurohyperforin isomer (**6**) (Hashida et al., 2010), furohyperforin isomer (**7**) (Hashida et al., 2010), hyperfol F (**8**) (Lou et al., 2020), (2*R*,3*R*,4*S*,6*R*)-6-methoxycarbonyl-3-methyl-4,6-di(3-methyl-2-butenyl)-2-(2-methyl-1-oxopropyl)-3-(4-methyl-3-pentenyl)cyclohexanone (**9**) (Verotta et al., 2000), and (2*R*,3*R*,4*S*,6*R*)-3-methyl-4,6-di(3-methyl-2-butenyl)-2-(2-meth yl-1-oxopropyl)-3-(4-methyl-3- pentenyl)cyclohexanone (**10**) (Verotta et al., 2000).

Hyperforen A (**2**) was obtained as colorless oil. Its molecular formula was fixed as $C_{34}H_{54}O_4$ based on ^{13}C NMR and HR-ESI-MS (high resolution electrospray ionization mass spectroscopy) data (*m*/*z* 549.3918, $[M + Na]^+$), indicating eight degrees of unsaturation. The infrared radiation (IR) spectrum of **2** exhibited strong absorption bands of the hydroxyl (3439 cm^{-1}) and carbonyl (1710 cm^{-1}) groups. The ^1H NMR spectrum of **2** (Table 2) showed the presence of three olefinic protons [δ_H 4.64 (d, J = 9.0 Hz), 4.69 (t, J = 7.2 Hz), and 4.99 (t, J = 7.2 Hz)] and two isopropyl groups. Combined with its HSQC and HMBC spectra, the ^{13}C NMR data of **2** (Table 2) revealed 34 signals, including three nonconjugated carbonyls and three nonconjugated double bonds. All the above evidence indicated that **2** was a PPAP derivative (Yang et al., 2014) containing a bicyclic system according to the remaining two degrees of unsaturation.

The planar structure of **2** was established by extensive analysis of its HSQC, ^1H–^1H COSY, and HMBC spectra (Fig. 4). In the HMBC spectrum, the correlations from Me-34 (δ_H 1.14) to C-8 (δ_C 41.6), C-9 (δ_C 47.2), and C-29 (δ_C 46.6), together with the ^1H–^1H COSY correlations of H-8/H-24/H-30/H_2-29, constructed a cyclopentane moiety (A-ring) with a methyl group at C-9. The correlations from Me-27 (δ_H 1.62, s) and Me-28 (δ_H 1.52, s) to C-26 (δ_C 131.3) and C-25 (δ_C 128.6), along with the ^1H–^1H COSY correlations of H-24/H-25 implied that an isobutenyl group is linked to C-24. Furthermore, a nine-membered carbon ring (B-ring) was assigned based on the HMBC correlations of H-1 (δ_H 3.85, s) to C-8 (δ_C 41.6), C-9 (δ_C 47.2), and C-2 (δ_C 201.3), H_2-14 to C-2 (δ_C 201.3), C-3 (δ_C 88.2), and C-4 (δ_C 210.3), and H_2-6 to C-4, as well as the proton spin system of H-20/H_2-19/H-5/H_2-6/H_2-7/H-8 in the ^1H–^1H COSY spectrum. In addition, a hydroxyl group at C-3 was defined from a proton of 3-OH (δ_H 4.35) to C-2, C-3, and C-4 in the HMBC spectrum. Likewise, the HMBC correlations from Me-17 (δ_H 1.59) and Me-18 (δ_H 1.64) to C-15 (δ_C 115.4) and C-16 (δ_C 137.1), and from Me-22 (δ_H 1.63) and Me-23 (δ_H 1.68) to C-20 (δ_C 121.7) and C-21 (δ_C 133.5) revealed that two prenyl groups were placed at C-3 and C-5, respectively. Finally, the HMBC correlations of H-1 (δ_H 3.85) and Me-12 (δ_H 0.98) to C-10 (δ_C 206.7) implied the linkage of isopropyl to C-1 through C-10. Thus, the planar structure of **2** was identified to be an unprecedented PPAP with a bicyclo[7.3.0]dodecane core. To the best of our knowledge, this PPAP represents the first PPAP with the largest pure carbon ring (a nine-membered carbocyclic system).

The relative configuration of compound **2** was determined by analysis of its ROESY spectrum (Fig. 4). The correlations of 3-OH/H-5, H-5/H-7β, H-7β/Me-34, Me-34/H-30, and H-30/H-24 revealed that those groups were on the same side of molecular and were randomly assigned as β-orientation. In addition, the ROESY correlations of H-14α/H-1 and H-1/H-8 indicated the α-orientation of these protons. Hence, the relative configuration of **2** was determined as depicted in Fig. 3.

Quantum chemical calculations were performed to further confirm the correctness of this compound. The ^{13}C NMR shielding constants of compound **2** were calculated with the GIAO method at the B3LYP/6–31 + g (d, p) level in chloroform with PCM. The computational ^{13}C NMR data were finally obtained using the linear regression analysis method, which was in good agreement with the experimental data (Table S4), with a correlation coefficient (R) of 0.9971 (Fig. 5A) (Xie et al., 2019). Finally, the absolute configuration of compound **2** was fixed by comparison of the experimental

Table 2 ^1H and ^{13}C NMR spectroscopic data of compound **2** in $CDCl_3$.

No.	δ_C, type	δ_H (J in Hz)	No.	δ_C, type	δ_H (J in Hz)
1	67.5, CH	3.85, s	18	25.9, CH_3	1.64, s
2	201.3, C		19*a*	25.4, CH_2	2.05, m
3	88.2, C		19*b*		2.26, m
4	210.3, C		20	121.7, CH	4.99, t (7.2)
5	47.1, CH	3.38, m	21	133.5, C	
6α	30.8, CH_2	1.08, m	22	18.14, CH_3	1.63, s
6β		1.18, m	23	25.83, CH_3	1.68, s
7α	31.1, CH_2	1.15, m	24	34.1, CH_2	2.15, m
7β		1.47, dd (15.6, 3.6)	25	128.6, CH	4.64, d (9.0)
8	41.6, CH	1.07, m	26	131.3, C	
9	47.2, C		27	25.8, CH_3	1.62, s
10	206.7, C		28	17.9, CH_3	1.52, s
11	42.7, CH	2.59, m	29	46.6, CH	1.23, dd (12.0, 3.6)
12	18.2, CH_3	0.98, d (6.6)	30	47.6, CH	0.96, m
13	18.5, CH_3	1.01, d (6.6)	31	27.8, CH	1.72, m
14*a*	33.4, CH_2	2.50, dd (15.6, 6.6)	32	15.9, CH_3	0.66, d (6.6)
14*b*		2.73, dd (15.6, 7.2)	33	21.4, CH_3	0.81, d (7.2)
15	115.4, CH	4.69, t (7.2)	34	12.3, CH_3	1.14, s
16	137.1, C		3-OH		4.35, s
17	18.19, CH_3	1.59, s			

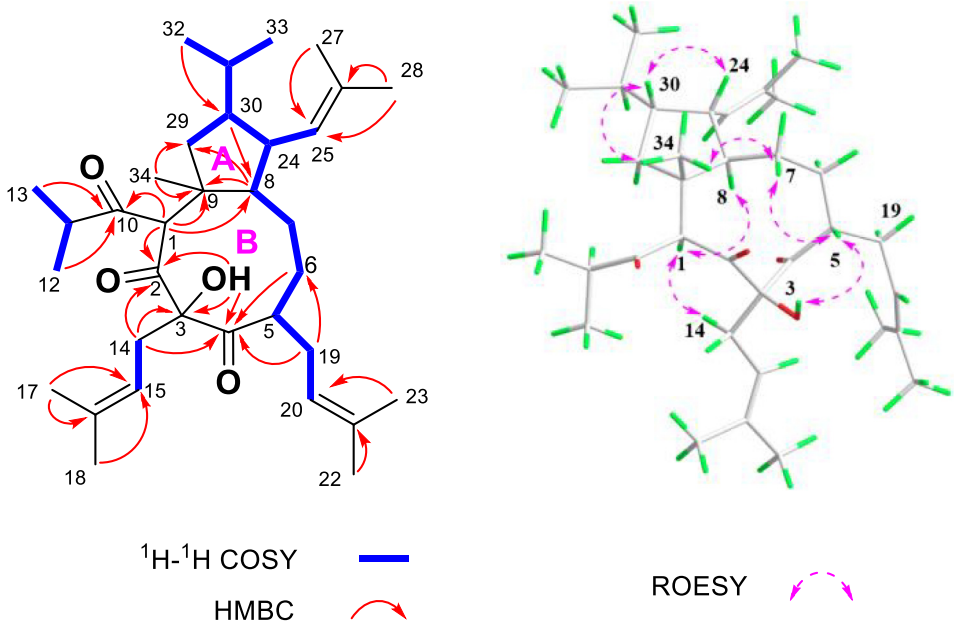

Fig. 4 HMBC, ^{1}H–^{1}H COSY, and ROESY correlations of **2**.

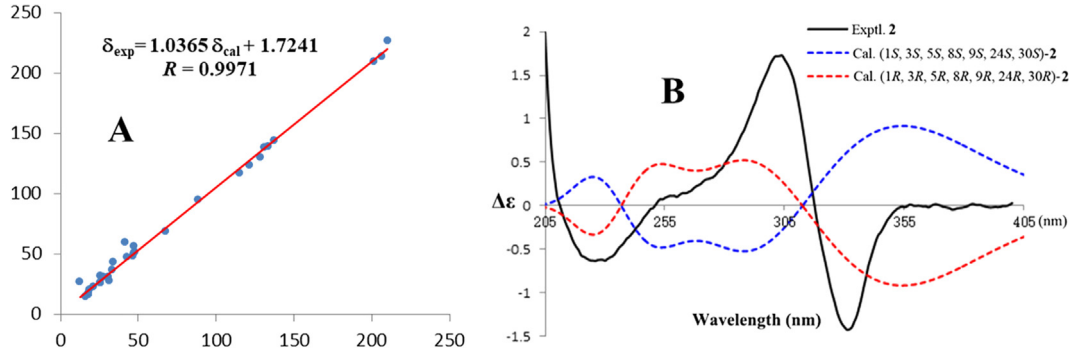

Fig. 5 (A) Regression analysis of the experimental versus alculated ^{13}C NMR chemical shifts of **2**. (B) Calculated and experimental ECD spectra of **2**.

and calculated ECD spectra (Zeng et al., 2018; Ma et al., 2017). The ECD spectra of (1*S*, 3*S*, 5*S*, 8*S*, 9*S*, 24*S*, 30*S*)-**2a** and (1*R*, 3*R*, 5*R*, 8*R*, 9*R*, 24*R*, 30*R*)-**2b** were calculated using time-dependent density functional theory (TDDFT) at the B3LYP-PCM/6–31 + G(d) levels with PCM in MeOH, and the calculated ECD spectra of **2b** matched well with the experimental ECD curve of **2** (Fig. 5B). Therefore, the absolute configuration of **2** was fixed as 1*R*, 3*R*, 5*R*, 8*R*, 9*R*, 24*R*, and 30*R* (Fig. 3).

3.1.4. Plausible biosynthetic pathway for 1–10

The plausible biosynthetic pathway for compounds **1**–**10** was proposed in Scheme 1 with hyperforin (**i**) as the precursor, which could be derived from 2,4,6-trihydroxybenzophenone *via* a cascade of isopentylation and intramolecular cyclization (Yang et al., 2018). The key intermediate (**i**) underwent an oxidation at C-3 and a hemiketal cyclization between OH-3 and a carbonyl of C-9 to obtain compound **1**, which further underwent a retrol aldol rearrangement to yield compound **3** (Verotta et al., 2000; Wang et al., 2019). A five-membered lactone ring of **3** was opened *via* hydrolysis, and the carboxylic group was lost to obtain compound **4**. Then, compound **4** underwent a double bond migration of the prenyl group (Liaw et al., 2019) and oxidation at the allylic methylene to the obtain key intermediate **iii**. Then, the hydroxyl was lost to get a carbonium ion at C-29, which underwent a Westphalen rearrangement (Blunt et al., 1964) to get the intermediate **v** with a carbonium ion at C-8. This intermediate further underwent a Wagner-Meerwein rearrangement to get intermediate **vi** (Li et al., 2005; Arriola et al., 2020; Yang and Grossman, 2020). Then, a new carbonium ion at the allylic methylene formed to yield **vii**, followed by a Wagner-Meerwein rearrangement and cyclization between the two prenyls to get compound **2**. Moreover, compound **5** was obtained *via* oxidation of the C-15, C-16 double bond of intermediate **i** and intramolecular cyclization between OH-2 and OH-15. Intermediate **ii** could be easily obtained from **i** through keto-enol tautomerism, which was further transformed into **6** and **7** by the same procedures as that of compound **5**. Similarly, intermediate **ii** was converted to **8** *via* oxidation of the C-20,

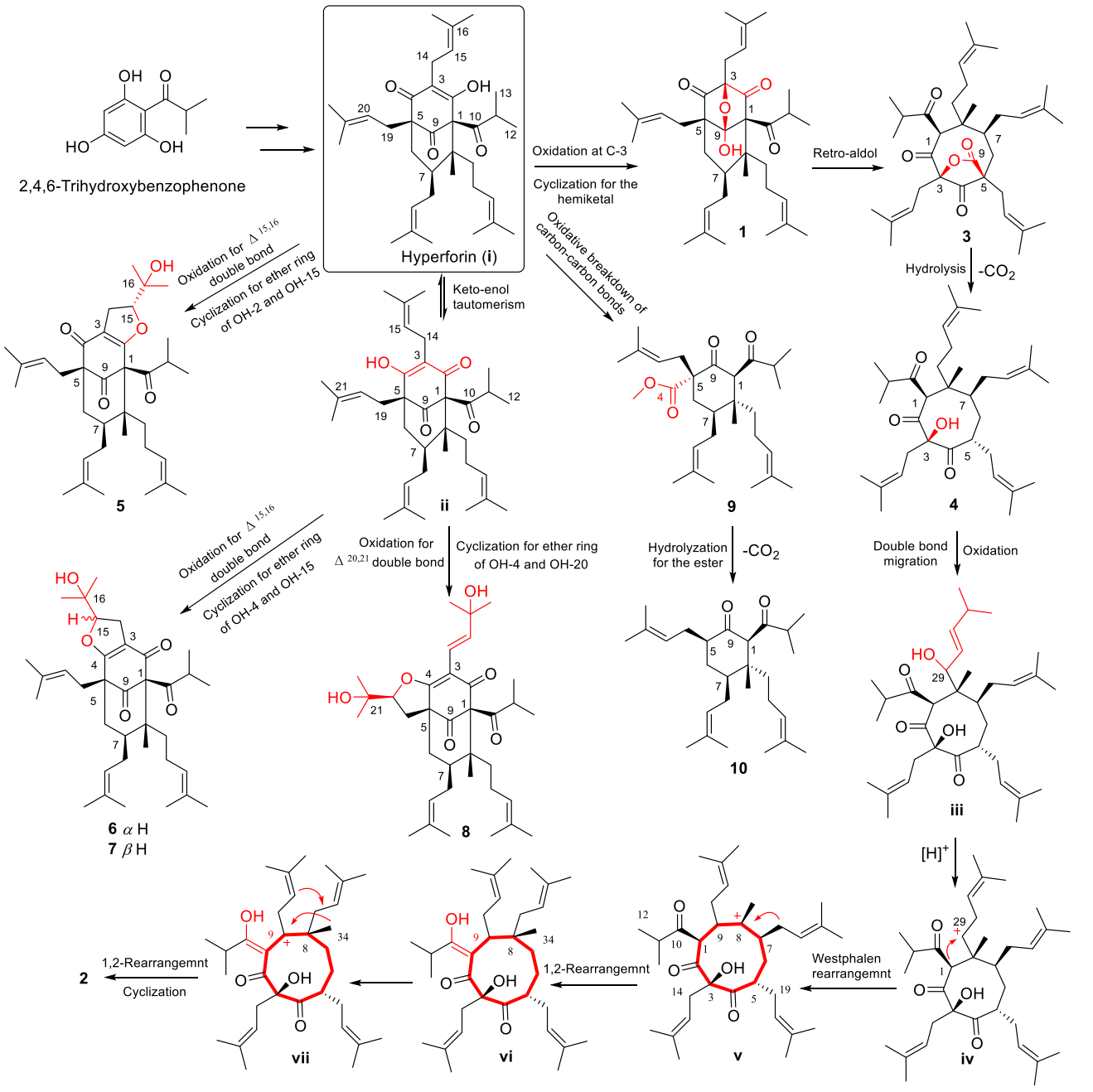

Scheme 1 Plausible biosynthetic pathway to **1**–**10.**

C-21 double bond and intramolecular cyclization between OH-4 and OH-20. In addition, compound **9** could be obtained by the oxidative breakdown of the C-1-C2 and C-3-C-4 carbon–carbon bonds of intermediate **i**, which underwent hydrolyzation of the ester and decarboxylation to get compound **10**.

3.2. Neuroprotective effects of the isolates against CORT-induced injury in PC12 cells

The isolates (**1**–**10**) were evaluated for their neuroprotective effects against CORT-induced injury in PC12 cells *via* the MTT method (Zhou et al., 2016; Jiang et al., 2014). The results showed that compounds **1**–**3**, **6**, and **10** showed neuroprotective effects against CORT-induced injury in PC12 cells at 20 μM (Fig. 6A). Then, those active compounds were tested for neuroprotective activity at three different concentrations (20 μM, 10 μM, and 5 μM). The results revealed that all these tested compounds were active at 10 μM. In particular, compound **3** exhibited the best neuroprotective effect in a dose-dependent manner, with a cell viability of 64.1% at 5 μM (Fig. 6B). The structural difference between compounds **3** and **1** is the presence of a five-membered lactone ring in compound **3**, and thus, this lactone ring may play a critical role in enhancing the neuroprotective activity. For the single ring PPAPs (**9** and **10**), the absence of a methyl ester (**10**) improved the activity. Compound **6** showed desired neuroprotective

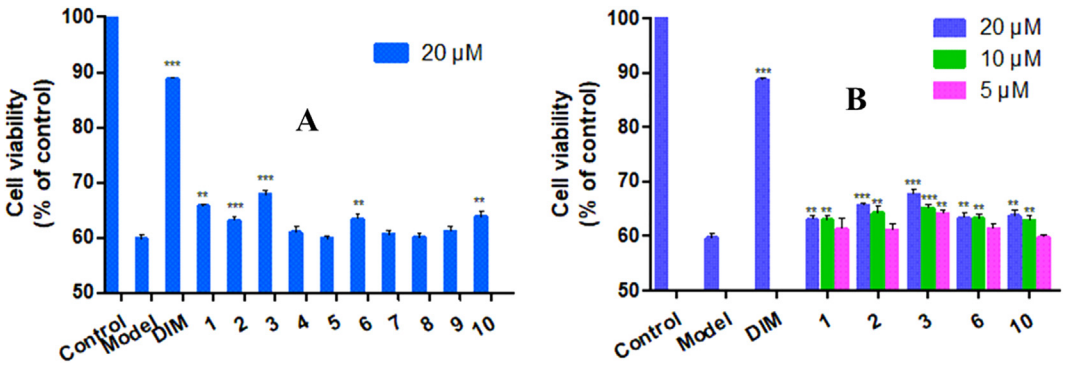

Fig. 6 (A) Neuroprotective effect of **1**–**10** against CORT-induced injury in PC12 cell at 20 μM; (B) Neuroprotective effect of compounds **1**–**3, 6,** and **10** at 5 μM, 10 μM, and 20 μM. ***$P < 0.001$, **$P < 0.01$, *$P < 0.05$ *vs*. model; Desipramine (DIM) is positive control.

activity when the 2-hydroxypropan-2-yl group on the furohyperforin was *β*-oriented, while compounds **5** and **7** with an *α*-oriented 2-hydroxypropan-2-yl group on the furohyperforin were inactive. This observation is contradictory for compound **8**, which had a *β*-oriented 2-hydroxypropan-2-yl group on the furohyperforin. This may be attributed to the hydroxyl group on a prenyl that decreased the activity.

4. Conclusions

In summary, bioassay and UPLC-Q-Orbitrap-MS/MS guided isolation of *H. perforatum* led to the isolation and identification of an unprecedented PPAP (**2**) and nine known PPAPs (**1**, **3**–**10**). To the best of our knowledge, compound **2** represents the first PPAP with an unprecedented bicyclo[7.3.0]dodecane core and the largest carbon ring. Compounds **1** (10.1‰) and **3** (2.0‰) were the main constituents of the extracts of this plant. Moreover, compounds **1**–**3**, **6**, and **10** (10 μM) showed neuroprotective protective effects against CORT-induced injury in PC12 cells. Findings from the current research suggest that **1** and **3** might be one of the major antidepressant active constituents for the extracts of *H. perforatum*. This investigation supports the therapeutic potential of SJW crude extracts with PPAPs as the active constituents for the prevention and treatment of depression.

CRediT authorship contribution statement

Huayong Lou: Writing – original draft. **Fengwei Ma:** Writing – original draft. **Ping Yi:** . **Zhanxing Hu:** Writing – original draft. **Wei Gu:** Writing – review & editing. **Liejun Huang:** Writing – review & editing. **Wenwen He:** Writing – review & editing. **Chunmao Yuan:** Funding acquisition, Methodology, Writing – review & editing. **Xiaojiang Hao:** Project administration, Supervision, Methodology, Writing – review & editing.

Declaration of Competing Interest

The authors declare that they have no known competing financial interests or personal relationships that could have appeared to influence the work reported in this paper.

Acknowledgements

This research was financially supported by the Science and Technology Department of Guizhou Province (QKH 2020-1Z076), the National Natural Science Foundation of China (NSFC, 31960087, U1812403, and 81760630), the 13th Batch of Outstanding Young Scientific and Technological Talents in Guizhou Province (QKHPTRC [2021]5633), the Science and Technology Plan of Guizhou Province (Grant No. QKHZC [2018]2824), High-level Innovative Talents in Guizhou Province (Thousand Levels of Talent for Chunmao Yuan in 2018), Cultivation project of National Natural Science Foundation of Guizhou Medical University (For Chunmao Yuan), and "Light of the West" Talent Cultivation Program of Chinese Academy of Sciences for Chunmao Yuan (RZ [2020]82).

Appendix A. Supplementary data

Supplementary data to this article can be found online at https://doi.org/10.1016/j.arabjc.2022.104057.

References

Ang, C.Y.W., Hu, L.H., Heinze, T.M., Cui, Y.Y., Freeman, J.P., Kozak, K., Luo, W.H., Liu, F.F., Mattia, A., Dinovi, M., 2004. Instability of St. John's Wort (*Hypericum perforatum* L.) and degradation of hyperforin in aqueous solutions and functional beverage. J. Agric. Food. Chem. 52, 6156–6164.

Arriola, K., Guarino, S., Schlawis, C., Arif, M.A., Colazza, S., Peri, E., Schulz, S., Millar, J.G., 2020. Identification of brassicadiene, a diterpene hydrocarbon attractive to the invasive stink bug bagrada hilaris, from volatiles of cauliflower seedlings *Brassica oleracea* var. botrytis. Org. Lett. 22, 2972–2975.

Besen, B.S., Balcl, O., Gunesoglu, C., Orhan, M., Somuncuoglu, E.I., Tatll, I.I., 2017. Obtaining medical textiles including microcapsules of the ozonated vegetable oils. Fiber. Polym. 18, 1079–1090.

Blunt, J.W., Hartshorn, M.P., Jones, F.W., Kirk, D.N., 1964. The westphalen rearrangement. Tetrahedron Lett. 22, 1399–1402.

Bruni, R., Pellati, F., Bellardi, M.G., Benvenuti, S., Paltrinieri, S., Bertaccini, A., Bianchi, A., 2005. Herbal drug quality and phytochemical composition of *Hypericum perforatum* L. affected by ash yellows phytoplasma infection. J. Agric. Food. Chem. 53, 964–968.

Cui, Y.Y., Catharina, W., 2002. Supercritical fluid extraction and high-performance liquid chromatographic determination of phloroglucinols in St. John's Wort (*Hypericum perforatum* L.). J. Agric. Food. Chem. 50, 2755–2759.

Cervo, L., Rozio, M., Ekalle-Soppo, C.B., Guiso, G., Morazzoni, P., Caccia, S., 2002. Role of hyperforin in the antidepressant-like activity of *Hypericum perforatum* extracts. Psychopharmacology 164, 423–428.

Chen, D.L., Sun, Z.C., Liu, Y.Y., Li, Z.Y., Liang, H.Q., Chen, L., Xu, X.D., Yang, J.S., Ma, G.X., Huo, X.W., 2020. Eleucanainones A and B: two dimeric structures from the bulbs of *Eleutherine americana* with anti-MRSA activity. Org. Lett. 9, 3449–3453.

Chen, M.H., He, X., Sun, H., Sun, Y., Li, L., Zhu, J.Y., Xia, G.Q., Guo, X., Zang, H., 2022. Phytochemical analysis, UPLC-ESI-Orbitrap-MS analysis, biological activity, and toxicity of extracts from *Tripleurospermum limosum* (Maxim.) Pobed. Arabian J. Chem. 15, 103797.

Evans-Lacko, S., Aguilar-Gaxiola, S., Al-Hamzawi, A., Alonso, J., Benjet, C., Bruffaerts, R., Chiu, W.T., Florescu, S., Girolamo, G. D., Gureje, O., Haro, J.M., He, Y., Hu, C., Karam, E.G., Kawakami, N., Lee, S., Lund, C., Kovess-Masfety, V., Levinson, D., Navarro-Mateu, F., Pennell, B.E., Sampson, N.A., Scott, K. M., Tachimori, H., Have, M.T., Viana, M.C., Williams, D.R., Wojtyniak, B.J., Zarkov, Z., Kessler, R.C., Chatterji, S., Thornicroft, G., 2018. Socio-economic variations in the mental health treatment gap for people with anxiety, mood, and substance use disorders: results from the WHO World Mental Health (WMH) surveys. Psychol. Med. 48, 1560–1571.

Food and Drug Administration (FDA) https://www.fda.gov/consumers/consumer-updates/depression-fda-approved-medications-may-help.

Germ, M., Stibilj, V., Kreft, S., Gaberščik, A., Kreft, I., 2010. Flavonoid, tannin and hypericin concentrations in the leaves of St. John's wort (*Hypericum perforatum* L.) are affected by UV-B radiation levels. Food Chem. 122, 471–474.

Germ, M., Stibilj, V., Kreft, S., Gaberščik, A., Pajk, F., Kreft, I., 2009. Selenium concentration in St. John's wort (*Hypericum perforatum* L.) herb after foliar spraying of young plants under different UV-B radiation levels. Food Chem. 117, 204–206.

Guo, Y., Zhang, N., Chen, C.M., Huang, J.F., Li, X.N., Liu, J.J., Zhu, H.C., Tong, Q.Y., Zhang, J.W., Luo, Z.W., Xue, Y.B., Zhang, Y. H., 2017. Tricyclic polyprenylated acylphloroglucinols from St John's Wort, *Hypericum perforatum*. J. Nat. Prod. 80, 1493–1504.

Hammer, K.D.P., Hillwig, M.L., Solco, A.K.S., Dixon, P.M., Delate, K., Murphy, P.A., Wurtele, E.S., Birt, D.F., 2007. Inhibition of prostaglandin E2 production by anti-inflammatory *Hypericum perforatum* extracts and constituents in RAW264.7 mouse macrophage cells. J. Agric. Food. Chem. 55, 7323–7331.

Hanwell, M.D., Curtis, D.E., Lonie, D.C., Vandermeersch, T., Zurek, E., Hutchison, G.R., 2012. Avogadro: an advanced semantic chemical editor, visualization, and analysis platform. J. Cheminf. 4, 17.

Hashida, C., Tanaka, N., Kashiwada, Y., Ogawa, M., Takaishi, Y., 2010. Prenylated phloroglucinol derivatives from *Hypericum perforatum* var. angustifolium. Chem. Pharm. Bull. 40, 1164–1167.

Hou, X.D., Guan, X.Q., Cao, Y.F., Weng, Z.M., Hu, Q., Liu, H.B., Jia, S.N., Zang, S.Z., Zhou, Q., Yang, L., Ge, G.B., Hou, J., 2020. Inhibition of pancreatic lipase by the constituents in St. John's Wort: In vitro and in silico investigations. Int. J. Biol. Macromol. 145, 620–633.

Hosni, K., Msaada, K., Taarit, M.B., Marzouk, B., 2017. Fatty acid composition and tocopherol content in four Tunisian *Hypericum* species: *Hypericum perforatum*, *Hypericum tomentosum*, *Hypericum perfoliatum* and *Hypericum ericoides* Ssp. *Roberti*. Arabian J. Chem. 10, S2736–S2741.

Hsu, F.F., 2021. Electrospray ionization with higher-energy collision dissociation tandem mass spectrometry toward characterization of ceramides as $[M + Li]^+$ ions: mechanisms of fragmentation and structural identification. Anal. Chim. Acta. 1142, 221–234.

Jiang, B.P., Liu, Y.M., Le, L., Li, Z.Y., Si, J.Y., Liu, X.M., Chang, Q., Pan, R.L., 2014. Cajaninstilbene acid prevents corticosterone-induced apoptosis in PC12 cells by inhibiting the mitochondrial apoptotic pathway. Cell Physiol. Biochem. 34, 1015–1026.

Kim, Y.H., Im, A.R., Park, B.K., Paek, S.H., Choi, G., Kim, Y.R., Whang, W.K., Lee, K.H., Oh, S.E., Lee, M.Y., 2018. Antidepressant-like and neuroprotective effects of ethanol extract from the root bark of Hibiscus syriacus L. BioMed Res. Int. 2018, 7383869.

Laakmann, G., Schule, C., Baghai, T., Kieser, M., 1998. St. John's Wort in mild to moderate depression: The relevance of hyperforin for the clinical efficacy. Pharmacopsychiatry 31, 54–59.

Liaw, C.C., Chang, J.L., Wang, B.W., Chen, P.L., Weng, J.R., Lin, K. W., Lin, C.N., 2019. Discovering a racemate polycyclic prenylated acylphloroglucinol with unprecedented skeleton by an ESI-LCMS analytical approach. Org. Lett. 21, 857–861.

Li, R.T., Xiao, W.L., Shen, Y.H., Zhao, Q.S., Sun, H.D., 2005. Structure characterization and possible biogenesis of three new families of nortriterpenoids: schisanartane, schiartane, and 18-norschiartane. Chem. Eur. J. 11, 2989–2996.

Li, L.C., Yin, Y., Zheng, G.M., Liu, S.G., Zhao, C., Ma, L.S., Shan, Q., Dai, X.X., Wei, L.T., Lin, J.W., Xie, W.P., 2022. Determining *β*-lactam antibiotics in aquaculture products by modified QuEChERS combined with ultra-high performance liquid chromatography-tandem mass spectrometry (UHPLC-MS/MS). Arabian J. Chem. 15, 103912.

Liu, T.T., Wu, H.B., Zhang, J., Deng, W.J., Yang, L.W., 2020. Modified eremophilanes from *Parasenecio hastatus* and their neuroprotective activities. J. Nat. Prod. 83, 185–193.

Lou, H.Y., Yi, P., Hu, Z.X., Li, Y.N., Zeng, Y.R., Gu, W., Huang, L. J., Yuan, C.M., Hao, X.J., 2020. Polycyclic polyprenylated acylphloroglucinols with acetylcholinesterase inhibitory activities from *Hypericum perforatum*. Fitoterapia 143, 104550.

Lou, H.Y., Zhang, Y., Ma, X.P., Jiang, S., Wang, X.P., Yi, P., Liang, G.Y., Wu, H.M., Feng, J., Jin, F.Y., Pan, W.D., 2018. Novel sesquiterpenoids isolated from *Chimonanthus praecox* and their antibacterial activities. Chin. J. Nat. Med. 16, 621–627.

Ma, F.W., Lou, H.Y., Ge, Y.H., Li, J.Y., Chen, C., Xu, S., Tang, L., Pan, W.D., 2021. Non-targeted analysis of vulgarisins by using collisional dissociation mass spectrometry for the discovery of analogues from *Prunella vulgaris*. Anal. Bioanal. Chem. 413, 6513–6521.

Ma, F.W., Xia, B., Luo, S.H., Li, S.H., Zhou, Y., 2016. Analysis of the lithiated leucosceptroids from *Leucosceptrum canum* to facilitate their identification and differentiation by electrospray ionization tandem mass spectrometry. Rapid Commun. Mass Sp. 30, 100–110.

Ma, X.P., Zhang, W.F., Yi, P., Lan, J.J., Xia, B., Jiang, S., Lou, H.Y., Pan, W.D., 2017. Novel flavones from the root of *Phytolacca acinosa* Roxb. Chem. Biodivers. 14, e1700361.

Sapolsky, R.M., 2000. The possibility of neurotoxicity in the hippocampus in major depression: a primer on neuron death. Biol. Psychiat. 8, 755–765.

Shadfar, S., Kim, Y.G., Katila, N., Neupane, S., Ojha, U., Bhurtel, S., Srivastav, S., Jeong, G.S., Park, P.H., Hong, J.T., Choi, D.Y., 2018. Neuroprotective effects of antidepressants via upregulation of neurotrophic factors in the MPTP model of parkinson's disease. Mol. Neurobiol. 55, 554–566.

Verotta, L., Appendino, G., Jakupovic, J., Bombardelli, E., 2000. Hyperforin analogues from St. John's Wort (*Hypericum perforatum*). J. Nat. Prod. 63, 412–415.

Wang, Y.L., Ye, Y.S., Fu, W.W., Wu, R., Xiang, Q., Lao, Y.Z., Yang, J.L., Tan, H.S., Yang, X.W., Yang, B.C., Xu, H.X., Xu, G., 2019. Garsubelone A, the first dimeric polycyclic polyprenylated acylphloroglucinols with complicated heptacyclic architecture from *Garcinia subelliptica*. Org. Lett. 21, 1534–1537.

Wilhelm, K.P., Biel, S., Siegers, C.P., 2001. Role of flavonoids in controlling the phototoxicity of *Hypericum perforatum* extracts. Phytomedicine 8, 306–309.

Xie, C.L., Chen, R.Z., Yang, S.H., Xia, J.M., Zhang, G.Y., Chen, C. H., Zhang, Y.D., Yang, X.W., 2019. Nesteretal A, a novel class of cage-like polyketide from marine-derived actinomycete *Nesterenkonia halobia*. Org. Lett. 21, 8174–8177.

Yang, D., Chen, M., Russo-Neustadt, A., 2012. Antidepressants are neuroprotective against nutrient deprivation stress in rat hippocampal neurons. Eur. J. Neurosci. 36, 2573–2587.

Yang, X.W., Ding, Y.Q., Zhang, J.J., Liu, X., Yang, L.X., Li, X.N., Ferreira, D., Walker, L.A., Xu, G., 2014. New acylphloroglucinol

derivatives with diverse architectures from *Hypericum henryi*. Org. Lett. 16, 2434–2437.

Yang, X.W., Grossman, R.B., Xu, G., 2018. Research progress of polycyclic polyprenylated acylphloroglucinols. Chem. Rev. 118, 3508–3558.

Yang, X.W., Grossman, R.B., 2020. Revision of the structure of hypatulone A by NMR, computations, and biosynthetic considerations. Org. Lett. 22, 760–763.

Zeng, Y.R., Yi, P., Gu, W., Xiao, C.X., Huang, L.J., Tian, D.S., Yan, H., Chen, D.Z., Yuan, C.M., Hao, X.J., 2018. Hypermonins A and B, two 6-norpolyprenylated acylphloroglucinols with unprecedented skeletons from Hypericum monogynum. Org. Biomol. Chem. 16, 4195–4198.

Zhao, W.Y., Yan, J.J., Zhang, M., Wang, C., Feng, L., Lv, X., Huo, X.K., Sun, C.P., Chen, L.X., Ma, X.C., 2021. Natural soluble epoxide hydrolase inhibitors from *Inula britanica* and their potential interactions with soluble epoxide hydrolase: Insight from inhibition kinetics and molecular dynamics. Chem-Biol. Interact. 345, 109571.

Zhou, Z.B., Li, Z.R., Wang, X.B., Luo, J.G., Kong, L.Y., 2016. Polycyclic polyprenylated derivatives from *Hypericum uralum*: neuroprotective effects and antidepressant-like activity of uralodin A. J. Nat. Prod. 5, 1231–1240.

Zou, Y.P., Lu, Y.H., Wei, D.Z., 2004. Antioxidant activity of a flavonoid-rich extract of *Hypericum perforatum* L. in vitro. J. Agric. Food. Chem. 52, 5032–5039.